Topographic Correction for Landsat 8 OLI Vegetation Reflectances Through Path Length Correction: A Comparison Between Explicit and Implicit Methods

Gaofei Yin, *Member, IEEE,* Lei Ma, Wei Zhao, *Senior Member, IEEE,* Yelu Zeng, *Member, IEEE,* Baodong Xu, and Shengbiao Wu

***Abstract*— Topographic correction is a prerequisite for generating radiometrically consistent Landsat 8 OLI vegetation reflectances in support of temporally continuous and spatially mosaicked applications. Path length correction (PLC) is a physically solid topographic correction method that avoids the involvement of any empirical parameter and is therefore suitable for reproducing the inherent reflectance of vegetation. This article compared two different implementation pathways of PLC, i.e., the explicit method (EM) and the implicit method (IM), which are based on the numerical inverse and analytical approximation of the PLC model, respectively. The results show that both EM and IM can obviously reduce the topographic effects on Landsat 8 OLI vegetation reflectances. EM performed slightly better than IM in eliminating the correlation between the topographic characteristics and the vegetation reflectances: the coefficient of determination between the green/red/ near-infrared (Nir) band reflectance and the local illumination was reduced from 0.257/0.148/0.467 for the uncorrected (UNCORR) case to 0.016/0.004/0.012 and 0.027/0.014/0.094 for the EM and IM corrected results, respectively. The coefficient of variation of the three band reflectances across different aspects was reduced from 16.5%/18.5%/18.7% for the UNCORR case to 3.2%/1.8%/0.9% and 5.3%/7.1%/7.3% for the EM and IM corrected results, respectively. In addition, the intraclass reflectance variability was also reduced after both the EM and IM corrections. Nevertheless, due to the ill-posed nature of the numerical inverse process, EM cannot fully reproduce the inherent vegetation reflectances, and the reflectances after topographic correction overestimated the inherent vegetation values. In contrast, the IM can achieve an appropriate tradeoff between topographic effect elimination and vegetation inherent reflectance preservation. In addition, IM is computationally very efficient compared to EM: using an ordinary laptop, IM can finish the topographic correction for a Landsat OLI image within several seconds, while this would take more than 20 h for EM. This article highlights the potential of using IM for generating radiometrically consistent Landsat 8 OLI vegetation reflectances.**

***Index Terms*— Explicit method (EM), implicit method (IM), path length correction (PLC), topographic correction.**

I. Introduction

THE Landsat series has provided the longest running terrestrial satellite record and has been widely used in land surface monitoring [1], [2]. One prerequisite for the proper application of Landsat data is the extraction of the intrinsic surface reflectance by correcting the confounding factors [3]. Over mountainous areas, topographic effects prominently contaminate the intrinsic surface reflectance and have negative impacts on the consistency of Landsat reflectances [4].

The topographic effects on Landsat reflectances have been recognized from the very early phase of Landsat application [5], [6], and many topographic correction methods can be found in the literature, e.g., CC [6], SCS [7], SCS + C [8], D-S [9], Minnaert [10], IC [11], and multiple forward mode (MFM) [12]–[14]. However, obvious discrepancies exist among these methods for improving the spatial, spectral, and temporal consistency of Landsat observations [15]. A proper topographic correction method should avoid empirical parameters, which are often temporally and spatially specific and cause inconsistency in topographically corrected images [4], [16].

Path length correction (PLC) is a novel and newly developed topographic correction method [17]–[19]. This method is based on the topographic effect on the distortion of the photon transferring path length within canopies: the path length is

Manuscript received May 23, 2019; revised October 30, 2019, February 17, 2020, March 14, 2020, and April 4, 2020; accepted April 11, 2020. Date of publication April 30, 2020; date of current version November 24, 2020. This work was supported in part by the GF6 Project under Grant 30-Y20A03-9003-17/18, in part by the National Natural Science Foundation of China under Grant 41971282 and Grant 41631180, in part by the Youth Innovation Promotion Association under Grant 2016333, and in part by the Fundamental Research Funds for the Central Universities. *(Corresponding author: Gaofei Yin.)*

Gaofei Yin is with the Faculty of Geosciences and Environmental Engineering, Southwest Jiaotong University, Chengdu 610031, China (e-mail: yingf@swjtu.edu.cn).

Lei Ma is with the School of Geography and Ocean Science, Nanjing University, Nanjing 210023, China, with the Jiangsu Provincial Key Laboratory of Geographic Information Science and Technology, Nanjing University, Nanjing 210023, China, and also with Signal Processing in Earth Observation, Technical University of Munich (TUM), 80333 Munich, Germany.

Wei Zhao is with the Institute of Mountain Hazards and Environment, Chinese Academy Sciences, Chengdu 610010, China, and also with the Key Laboratory of Geospatial Technology for Middle and Lower Yellow River Regions, Ministry of Education, Henan University, Kaifeng 475004, China.

Yelu Zeng is with the Department of Global Ecology, Carnegie Institution for Science, Stanford, CA 94305 USA.

Baodong Xu is with the Macro Agriculture Research Institute, College of Resources and Environment, Huazhong Agricultural University, Wuhan 430070, China.

Shengbiao Wu is with the Key Laboratory of Remote Sensing Science, Institute of Remote Sensing and Digital Earth, Chinese Academy of Sciences, Beijing 100101, China.

Color versions of one or more of the figures in this article are available online at https://ieeexplore.ieee.org.

Digital Object Identifier 10.1109/TGRS.2020.2987985

stretched and compressed by topography in the upslope and downslope directions, respectively [20], [21]. PLC has a solid physical basis and avoids the involvement of any empirical parameter.

The novel PLC paradigm for topographic correction can be implemented using two different methods, i.e., explicit method (EM) [18] and implicit method (IM) [17]. The EM was inspired by the MFM method [12]–[14] and obtains the topographically corrected reflectances through direct use of the PLC canopy reflectance model in the MFM. In contrast, IM simplifies the PLC canopy reflectance model to obtain a multiplicative conversion coefficient that can directly transfer the original reflectances to their equivalent values on horizontal surfaces [17]. Assessments revealed that both EM and IM outperform most other topographic correction methods [17], [18]. However, these two methods have not been systematically compared.

To evaluate the performance of topographic correction methods, many criteria have been proposed, including visual assessment, correlation between the reflectance and topographic characteristics (e.g., local illumination and aspect), reflectance variation for a given land cover type, and the improvement of the accuracy of land cover classification and biophysical parameter retrieval [22]. However, there is no consensus on which criterion is the most effective and objective. In fact, previous studies have revealed that different assessment criteria would provide different assessment results even for the same topographic correction method [15]. Therefore, multicriteria evaluation of topographic correction methods has been increasingly preferred in [15], [17], and [22].

The objective of this article is to compare the performance of EM and IM in the topographic correction of Landsat 8 OLI reflectances. In the comparison, multiple criteria were used to provide a systematic result. The mechanism of PLC for topographic correction and its implementation in EM and IM are described in Section II. The experimental setup for EM and IM comparison and the corresponding results are given in Sections III and IV, respectively. Finally, a discussion and conclusion are presented in Sections V and VI, respectively.

II. Methods

A. PLC for the Topographic Correction of Vegetation Reflectance

PLC was proposed based on the classic radiative transfer equation stating the interaction between light and leaves within canopies [23], [24]. To obtain its concise or even analytical solution, the bidirectional reflectance is often decomposed into single scattering and multiscattering components [25]. Here, we briefly introduce the modeling of single-order scattering from leaves, which is the key of our PLC method. The other two components of the complete radiative transfer process (i.e., single-order scattering from soil and multiple scattering) can be found in [18].

The reflectance from the single-order scattering of the vegetation (ρ_1^c) can be calculated as [25]

$$\rho_1^c = \frac{\Gamma(r_1, r_2)L}{\mu_1 \mu_2} \int_{-1}^{0} Q(r_1, r_2, z) dz \tag{1}$$

where L is the leaf area index (LAI); $\cos(\theta_1)$ and $\cos(\theta_2)$ are the polar angles of Ω_1 and Ω_2, respectively; and Q (Ω_1, Ω_2, z) is the bidirectional gap probability between Ω_1 and Ω_2 at a relative optical height of z, which can be computed as follows:

$$Q(r_1, r_2, z) = p(r_1, z)p(r_2, z)C_{\mathrm{HS}}(\gamma, z) \tag{2}$$

where $p(\Omega_1, z)$ and $p(\Omega_2, z)$ are the directional gap probabilities at height z in the solar and viewing directions, respectively. C_{HS} is the hotspot correction function used to account for the sharp reflectance increase close to the backscattering direction and can be formulated using an exponential model [25], [26].

In (2), the directional gap probability can be further calculated by Beer's law [27], [28], that is,

$$p(\theta, \varphi) = e^{G(\theta,\varphi)s(\theta,\varphi)L_z} \tag{3}$$

where L_z is the accumulated LAI from the top of the canopy to a height z; θ and φ are the zenith and azimuth angles, respectively, for the solar or viewing direction; and $s(\Omega)$ is the path length, i.e., the distance between z and the top of the canopy along the solar or viewing direction. For a canopy over a horizontal surface, the path length can be simply computed as a function of the solar/viewing zenith angle (θ) [18], that is,

$$S(\theta) = 1/\cos\theta. \tag{4}$$

Over a sloping surface, the path length is obviously influenced by the topography and can be formulized as

$$S_t(\theta, \varphi, \alpha, \beta) = \frac{1}{\cos\theta(1 - \tan\alpha\cos(\varphi - \beta)\tan\theta)} \tag{5}$$

where α and β are, respectively, the slope and aspect of the sloping surface.

Overall, the flowchart for the vegetation reflectance topographic correction using PLC can be summarized as follows. First, the vegetation reflectance is reformulated as an explicit function of the path length by means of the radiative transfer equation. Then, the path length parameterization for a horizontal surface [(4)] is replaced with that for a sloping surface [(5)]. Finally, the original reflectance over rugged terrain is normalized to the horizontally equivalent reflectance, i.e., the reflectance of a hypothetical canopy with identical leaf and soil optical properties and individual plant structure to the original canopy but on a horizontal surface (only changing the topological relationship between different plants). The normalization process can be implemented through EM and IM, detailed in Sections II-B and II-C.

B. EM

The EM was inspired by the MFM method proposed by Soenen *et al.* [14]. This method is based on the explicit application of canopy reflectance models in the MFM. Several canopy reflectance models have been employed in the MFM method, e.g., the Li–Strahler geometric-optical mutual shadowing (GOMS) model [14], [29], discrete anisotropic radiative transfer (DART) model [12], [30], and geometric-optical model for sloping terrains (the GOST model) [13], [31]. The EM under the PLC paradigm uses the PLC canopy reflectance model developed in our previous study [18].

TABLE I
DISTRIBUTION OF THE TOPOGRAPHY, CANOPY, LEAF, AND SOIL PARAMETERS USED IN THE PLC MODEL PARAMETERIZATION FOR EM TOPOGRAPHIC CORRECTION

	Parameter	Unit	Min	Max
Topography	Slope	°	0	70
	Aspect	°	0	360
Canopy	Leaf area index	m^2/m^2	0	8
	Averaged leaf inclination angle	°	35	80
	Hot spot size	Unitless	0.1	0.5
Leaf (simulated by the PROSPECT model)	Leaf chlorophyll content	$mg \cdot cm^{-2}$	20	90
	Leaf structure parameter	Unitless	1.2	2.2
	Leaf equivalent water thinness	$g \cdot cm^{-2}$	0.6	0.8
	Dry matter content	$g \cdot cm^{-2}$	0.003	0.02
Soil	Brightness parameter	Unitless	0.1	1.0

The EM obtains the topographically corrected reflectances through three main steps as follows.

1) *Parameterization*: Parameter combinations are randomly generated according to the given distributions; then, the corresponding reflectances are simulated through the PLC canopy reflectance model, and the parameter–reflectance pairs are tabulated as a lookup table (LUT).
2) *Inversion:* The canopy parameters (e.g., LAI, average leaf angle, and leaf and soil reflectances) are estimated through the above LUT from remote sensing imagery and a digital elevation model (DEM).
3) *Simulation:* The corrected reflectance is obtained through forward running of the PLC model under identical canopy parameters as the original case but over a horizontal surface (i.e., slope $= 0°$ and aspect $= 0°$) [18].

The generation of the LUT (i.e., parameterization of the PLC model) is the prerequisite for the EM. In this article, 100 000 parameter combinations were randomly generated following the uniform distributions summarized in Table I. To ensure generality, relatively wide dynamic ranges were adopted. It is worth noting that the leaf optical properties used for the PLC model were simulated through the PROSPECT model [32], in which the leaf optical properties are expressed as a function of the leaf chlorophyll content ($mg \cdot cm^{-2}$), leaf structure parameter (unitless), leaf equivalent water thickness ($g \cdot cm^{-2}$), and dry matter content ($g \cdot cm^{-2}$). The soil was characterized by a representative set of soil spectra (assumed to be Lambertian) multiplied by a brightness parameter [33]. Finally, the sun-target-sensor geometry can be determined according to the specific application scenario from the metafile of the remote sensing data.

The inversion and simulation procedures are relatively common and can be implemented according to similar studies in MFM, such as [12]–[14] and [18]. It is worth noting that the inversion procedure is by nature ill-posed, i.e., different input combinations can correspond to identical canopy reflectance [34], [35]. To mitigate the ill-posed problem, the multiple best solutions method was used in this article; specifically, we selected the 50 best solutions in the inversion procedure, and the mean of the reflectances generated in the simulation procedure was seen as the final corrected vegetation reflectance.

C. IM

Based on three main assumptions, i.e., 1) the canopy is illuminated by collimated light; 2) the radiance collected by the sensor is only from the single scattering of leaves; and 3) the leaf inclination distribution function is spherical, then the vegetation reflectance formulized by PLC (see Section II-A) can be tremendously simplified as [17]

$$\rho = \frac{2\Gamma(\Omega_1 \rightarrow \Omega_2)}{\cos(\theta_1)\cos(\theta_2)} \frac{1}{S(\Omega_1) + S(\Omega_2)} \tag{6}$$

where θ_1 and θ_2 are the solar and viewing zenith angles, respectively and $S(\Omega_1)$ and $S(\Omega_2)$ are the path lengths along the solar and viewing directions, respectively.

The radiometrically consistent definition of vegetation bidirectional reflectance is critical for modeling and correcting the vegetation reflectance over rugged terrains [36]. This value can be defined as the ratio of vegetation reflected radiance to the incident irradiance on the slope, as in [37] and [38]. Alternatively, this value can also be defined as the ratio of

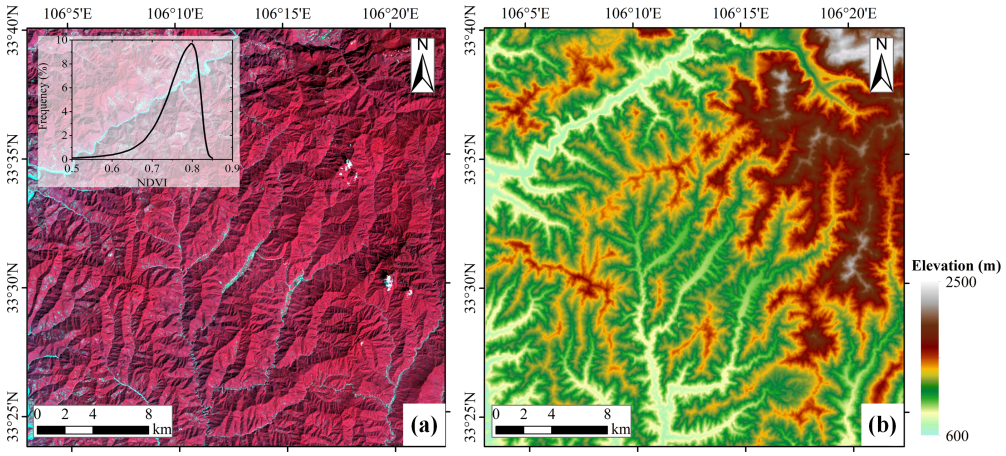

Fig. 1. Study area. (a) Landsat 8 OLI image shown with combinations of Nir, red, and green bands. (b) Elevation map. The inset in (a) shows the frequency distribution of the NDVI.

the vegetation reflected radiance to the incident irradiance on the horizontal surface. The MFM series often adopts the latter definition, such as the definition in [12]–[14] and [17]. Both the EM and IM in this article employed the latter definition, which makes the sun-target-observation geometries for reflectances over rugged and corresponding horizontal surfaces identical. In addition, the leaf scattering phase functions $[\Gamma(\Omega_1 \rightarrow \Omega_2)]$ for rugged and corresponding horizontal surfaces are also the same because of the geotropic nature of plant growth [39], [40]. Therefore, in the simplified canopy reflectance formulation [(6)], only the term of $1/[S(\Omega_1)+S(\Omega_2)]$ is related to the topography.

The vegetation reflectances over the sloping (ρ_T) and corresponding horizontal terrains (ρ_{EM}) can both be expressed by (6), and the topographically independent variables, i.e., $\cos(\theta_1)$, $\cos(\theta_2)$, and $\Gamma(\Omega_1 \rightarrow \Omega_2)$, can be eliminated by dividing the two reflectances. We obtained the following formula for topographic correction:

$$\rho_{\mathrm{PLC}} = \rho_t \frac{S(\Omega_1) + S(\Omega_2)}{S_t(\Omega_1) + S_t(\Omega_2)} \tag{7}$$

where $S(\Omega_1)$ and $S(\Omega_2)$ are the path lengths along the solar and viewing directions, respectively, over flat terrain, and $S_t(\Omega_1)$ and $S_t(\Omega_2)$ are their counterparts over the sloping terrain. The path lengths over the horizontal and sloping terrains can be calculated by (4) and (5), respectively.

III. Experimental Setup

A. Study Area

The study area is centered at approximately 33° 32′ N and 106° 13′ E (Fig. 1), located in Lueyang County, Shaanxi, China. The study area covers approximately 30 km × 30 km with altitudes ranging between 600 and 2500 m above sea level [Fig. 1(b)]. The land cover types are relatively limited and dominated by forests.

B. Data

A Level 1 Landsat 8 operational land imager (OLI) image [Fig. 1(a)] with path and row of 129 and 37, respectively, acquired on September 6, 2017, was freely downloaded from the EarthExplorer platform (https://earthexplorer.usgs.gov/). The spatial resolution of the downloaded Landsat 8 OLI image is 30 m. Before topographic correction, the original 16-bit integer values in the Level 1 product were converted to top of atmosphere (TOA) reflectance using the multiplicative and additive scaling factors stored in the metadata [41]. Sun-target-observation geometries (including solar zenith angle, solar azimuth angle, viewing zenith angle, and viewing azimuth angle) are prerequisites for calculation of the path length [see (5) and (6)]. In this article, pixelwise values for sun-target-observation geometries were derived using the L8-angles package provided by the United States Geological Survey (USGS).

The slope and aspect, which are also used for calculation of the path length [see (5) and (6)], were derived from the advanced spaceborne thermal emission and reflectance radiometer (ASTER) global DEM (GDEM) version 2 product [42]. The ASTER GDEM was generated by the Ministry of Economy, Trade, and Industry (METI) in Japan and the National Aeronautics and Space Administration (NASA) in the United States. The spatial resolution is 1 arc-second (∼30 m), approximately the same as that of the Landsat 8 OLI image.

C. Method Assessment and Comparison

Comparisons between PLC and other methods were conducted in [17] and [18]. Therefore, this article focused on comparing the two pathways of the PLC methods, i.e., the IM and EM.

Topographic corrections by both the EM and IM were implemented for the abovementioned Landsat 8 OLI image, and the corresponding corrected reflectances were assessed and compared. Absolute correction accuracy is difficult to obtain because of the lack of referenced horizontal reflectances for sloping reflectances [13], [43]. Therefore, multicriteria evaluation is commonly recommended to provide a comprehensive evaluation result [15], [17], [22]. In this article, five criteria were adopted to assess the performance of topographic correction, i.e., 1) visual inspection; 2) analysis of reflectance dependence on the local illumination condition [$\cos(i)$]; and 3)

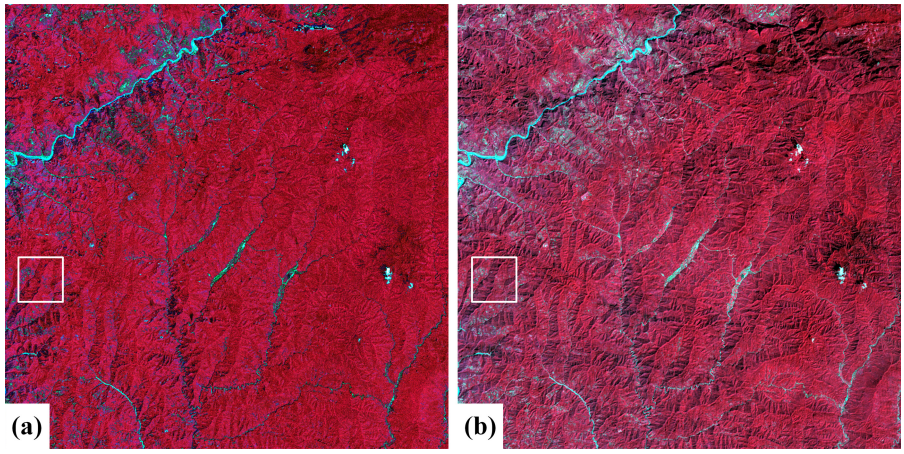

Fig. 2. False color composite images after topographic correction with (a) EM and (b) IM.

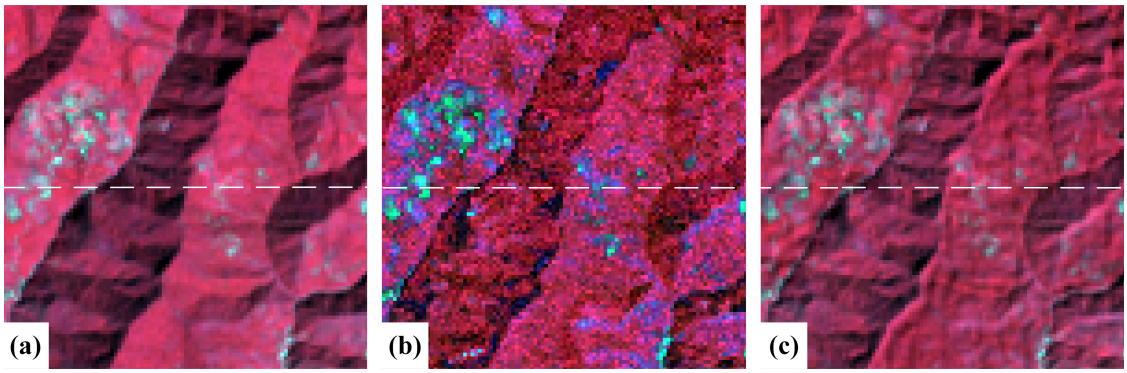

Fig. 3. Enlargement of the inset shown as a white box in Fig. 2. (a) Image before topographic correction. (b) Topographic correction with the EM. (c) Topographic correction with the IM. The dashed lines are the established profiles for the analysis of normalized reflectance in Fig. 4.

that on aspect; 4) reduction in intraclass reflectance variation; and 5) computational efficiency.

For visual inspection, a profile was established to analyze the change in the normalized reflectance after topographic correction. The normalized reflectance was calculated as $(\mathrm{Ref}_i - \mathrm{Ref}_a)/\mathrm{Ref}_a$, where Ref_i and Ref_a are the reflectance for the ith pixel and the averaged reflectance for the profile. The reflectance dependence on $\cos(i)$ and that on aspect are the two complementary criteria to analyze the reflectance variation caused by topography [13]. The reduction in intraclass variability was also a commonly used criterion, yet it suffers from high uncertainty embedded in the land cover classification over mountainous areas [44]. Therefore, the normalized difference vegetation index, which is insensitive to topographic effects, was often selected as a proxy of the land cover type [38], [45]. The NDVI of vegetation in our study area mainly spans from 0.7 to 0.82 [see the inset of Fig. 1(a)], so we separated the vegetation into six classes with a step of 0.02, and we numbered them in the order of increasing NDVI values. High computational efficiency is the prerequisite for operational implementation. The computational times for EM and IM, implemented by MATLAB R2018a on a laptop with an Intel Core i7-6500 2.5-GHz CPU and 8-GB RAM, was used as the proxy for computational efficiency.

IV. Results

The PLC method is band independent and therefore can be applied for every band of Landsat 8 OLI data. However, for brevity, only green, red, and near-infrared (Nir) bands are shown.

A. Visual Inspection

The original image [Fig. 1(a)] is characterized by a significant topographic effect. For example, sun-facing slopes are obviously brighter than shade slopes. Both EM and IM significantly reduced the topographic effect in the original image, yet with different levels. Intuitively, the reflectance variations with the topography almost disappeared after EM correction [Fig. 2(a)]. However, some local-scale reflectance variations with the topography can still be found in the IM corrected image [Fig. 2(b)].

A detailed visual inspection of the enlarged area (white box shown in Fig. 2) is shown in Fig. 3. The reflectance values for the sunny and shady slopes in the original image were remarkably decreased and increased, respectively, after correction, resulting in a more homogeneous scene. A closer inspection revealed that EM caused many artifacts, especially for the nonvegetation pixels [Fig. 3(b)]. In contrast, IM obtained a robust correction result without any artifacts.

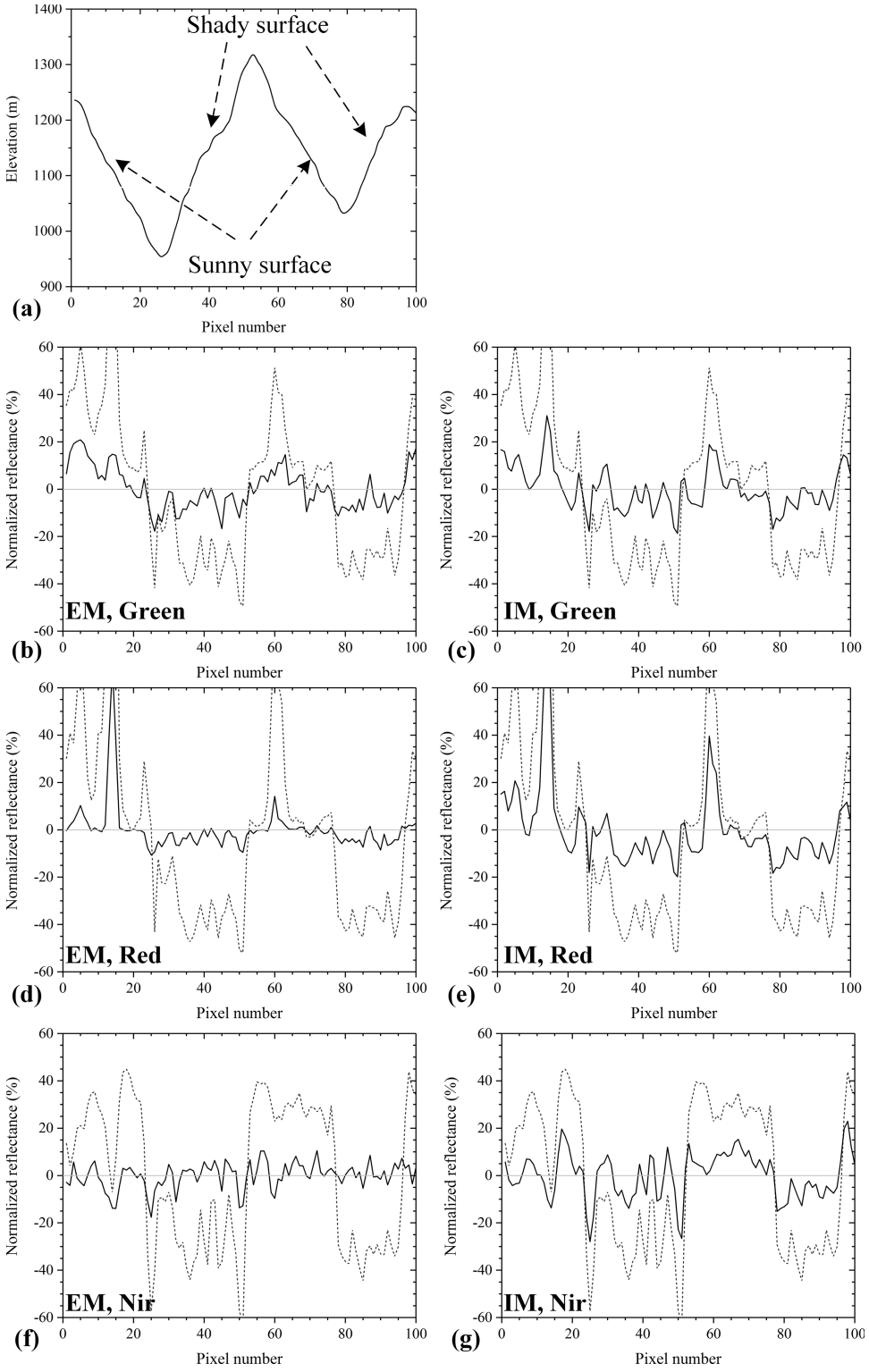

Fig. 4. Profiles of (a) elevation and (b)–(g) reflectance for the dashed lines in Fig. 3. Solid lines in (b)–(g) represent the normalized reflectance after topographic correction with (b), (d), and (f) EM and (c), (e), and (g) IM. Dashed lines represent those before correction. The second-to-fourth rows exhibit cases for green, red, and Nir bands in sequence. The normalized reflectance, defined as (ref−avef)/avef, where ref and avef are the reflectance and averaged reflectance, respectively, was used to reveal the reflectance variation regardless of its absolute magnitude.

The reflectance profiles for the lines in Fig. 3 are further exhibited in Fig. 4. These profiles cover two sunny (pixels 1–25 and 51–75) and two shady slopes (pixels 26–50 and 76–100) [Fig. 4(a)], which correspond to positive and negative values, respectively, for the uncorrected (UNCORR) normalized reflectance [dotted lines in Fig. 4(b)–(g)]. The dynamic range of the normalized reflectance was significantly reduced after topographic correction. The normalized

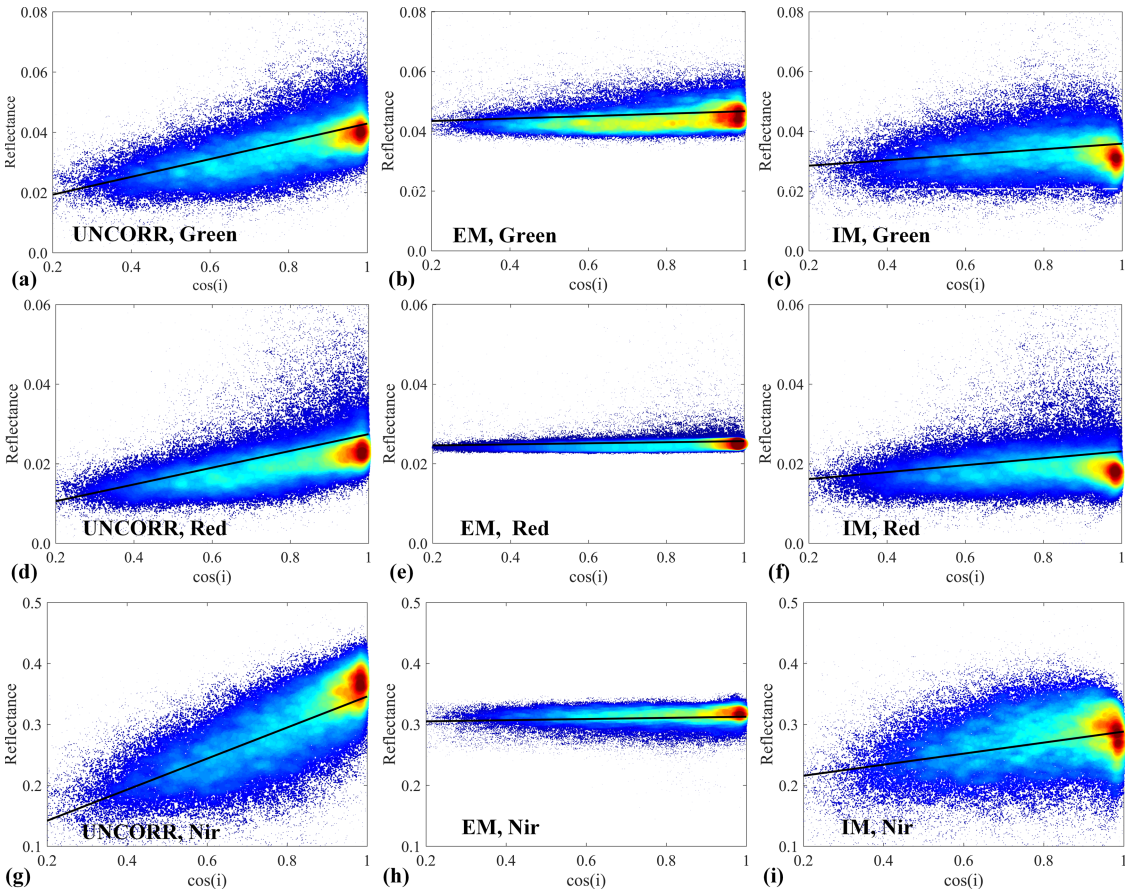

Fig. 5. Density scatterplots between the reflectance and the cosine of the local solar incidence angle [cos(i)]. The first-to-third rows exhibit cases for green, red, and Nir bands in sequence, and the first-to-third columns show cases for topographically UNCORR and corrected results from the EM and IM in sequence. The solid lines are the regressed results between reflectance and cos(i).

TABLE II

REGRESSION RESULTS BETWEEN THE REFLECTANCE (y) AND THE COSINE OF THE LOCAL SOLAR INCIDENCE ANGLE (x). LOWER VALUES OF THE SLOPE AND R^2 OF THE FITTED LINE INDICATE A BETTER CORRECTED RESULT

Correction method	Green band		Red band		Nir band	
	Regression function	R^2	Regression function	R^2	Regression function	R^2
Original image	y =0.030 x + 0.013	0.257	y = 0.021 x + 0.006	0.148	y = 0.255 x + 0.091	0.467
EM	y = 0.004 x + 0.043	0.016	y = 0.001 x + 0.024	0.004	y = 0.010 x + 0.303	0.012
IM	y = 0.009 x + 0.027	0.032	y = 0.009 x + 0.014	0.030	y = 0.091 x + 0.198	0.094

reflectance profile after EM correction was closer to 0 than that after IM correction, confirming the better topographic effect mitigation of EM than IM.

B. Dependence of Reflectances on Local Illumination Condition

Correlation analysis between the reflectance and the cosine of the local incident angle [cos(i)] is one of the key quantitative criteria to assess the performance of topographic methods. The correlation between the reflectance and cos(i) is shown in Fig. 5, and the detailed regression results are summarized in Table II. Significant positive correlations were observed for the original UNCORR image, especially in the Nir band (R^2 = 0.467 and slope of the regressed line = 0.225). Both EM and IM can obviously weaken the correlation: R^2 values for all the three bands were significantly decreased, and the regressed lines were inclined to be horizontal. Intuitively, EM performed better than IM in topographic effect mitigation because the R^2 and the slopes of the regressed lines from EM were all obviously lower than those from IM. However, closer inspection revealed that the reflectances after EM were shifted to higher values, indicating that EM may overestimate the "true" corrected reflectances. In addition, the reflectance dynamic range for a specific cos(i) for EM is narrower than those for the UNCORR and IM cases, i.e., EM may somewhat eliminate inherent surface information.

C. Dependence of Reflectances on Aspect

Topographic effects cause aspect dependence of reflectance, e.g., the sunny aspect appears higher than the shady aspect [46]. In Fig. 6, the red solid curves exhibit the reflectance variations across different aspect angles.

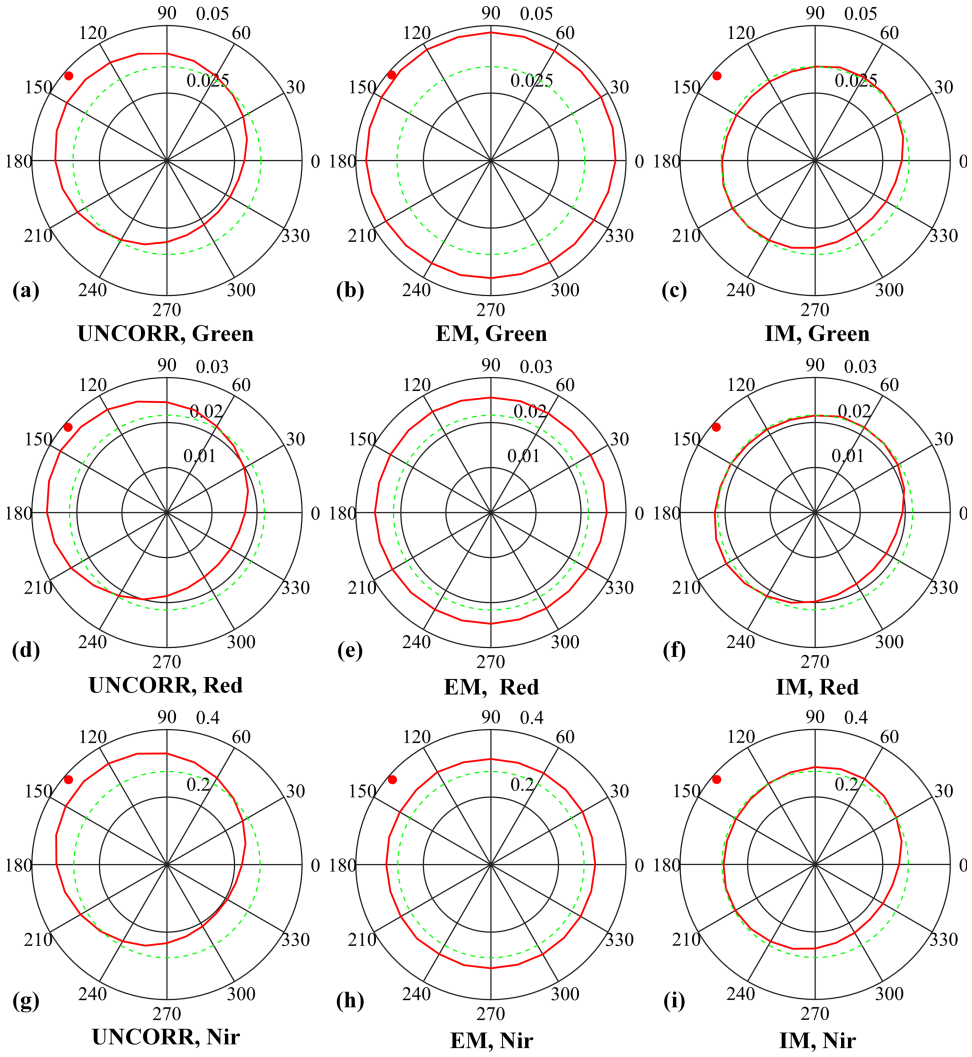

Fig. 6. Average reflectances across aspect angles. The first-to-third rows exhibit cases for the green, red, and Nir bands in sequence, and the first-to-third columns show cases for topographically UNCORR and corrected results from the EM and IM in sequence. The radius represents the magnitude of the reflectance with 0 in the center, and the polar angle represents the aspect. The red point in each plot represents the solar azimuth. The solid red curves show the real aspect distribution of the reflectances, and the dashed green curves are hypothetically aspect-free cases with the radius of the averaged UNCORR reflectances and centered in the ordinate origin. For a satisfactory correction method, the solid red and dashed green curves should coincide with each other.

For comparison, we also show the hypothetically aspect-free distribution of the reflectances (green dashed curves). The hypothetical cases are circles centered in the ordinate origin with a radius of the corresponding averaged UNCORR reflectances. The averaged UNCORR reflectances are seen as the ideal values of aspect-free reflectances because the sunny aspect-induced overestimation and shady aspect-induced underestimation would cancel each other throughout the study area; therefore, the averaged reflectances are not strongly influenced by the topography [22]. Because of the topographic effect, the curves of the UNCORR reflectance are flat ovals, which also shifted to sun-facing aspects (∼139.2°). After topographic correction by EM and IM, the reflectances became nearly aspect-free, and the curves are more similar to circles, especially for the EM cases.

The mean and coefficient of variation (CV, %) of reflectances across different aspects can be used to quantify the potential of topographic correction methods to preserve the land surface inherent reflectances and reduce the topographic effect, respectively (see Table III). Specifically, the more similar the mean of corrected reflectances is to that of the original reflectances, the better the method to preserve the surface inherent reflectances. The smaller the CV is, the better the method is able to reduce the topographic effect. As indicated by CV, EM can mitigate topographic effects very satisfactorily, and the CVs were reduced from 16.5%, 18.5%, and 18.7% for the UNCORR cases to 3.2%, 1.8%, and 0.9% after EM correction in the green, red, and Nir bands, respectively. IM performed somewhat worse than EM, with the CV reduced to 5.3%, 7.1%, and 7.3% in the corresponding bands. However, IM outperformed EM in preserving the inherent surface reflectances. For the IM cases, the inherent reflectance distortions were −2.9% [(0.033–0.034)/0.034], 4.5%, and 4.3% in the green, red, and Nir bands, respectively. These values were much better than those from the EM, i.e., 35.3%, 13.6%, and 12.3% in the corresponding bands.

TABLE III
MEAN AND CV OF REFLECTANCE ACROSS DIFFERENT ASPECTS

Correction method	Green band		Red band		Nir band	
	Mean	CV	Mean	CV	Mean	CV
Original image	0.034	16.5%	0.022	18.5%	0.276	18.7%
EM	0.046	3.2%	0.025	1.8%	0.310	0.9%
IM	0.033	5.3%	0.021	7.1%	0.264	7.3%

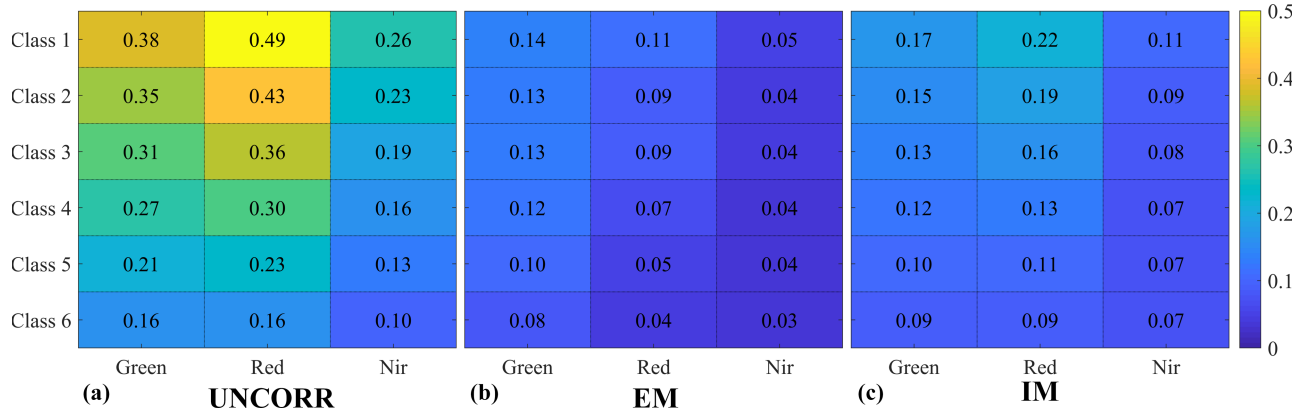

Fig. 7. CV of reflectance for six land cover classes at the green, red, and Nir bands (a) before correction and after correction by (b) EM and (c) IM.

D. Reduction in Intraclass Reflectance Variability

Intraclass reflectance should be homogenized after topographic correction. To quantify the reflectance variability within each class, we calculated the CV of reflectance before and after topographic correction (Fig. 7).

Before topographic correction [Fig. 7(a)], the intraclass variability is obvious, especially for sparse vegetation (with a small class number). This result may be because of the complexity of the architectural properties for sparse vegetation. In this case, in addition to the topographic effect, the background reflectance also contributes considerably to the canopy reflectance variation. In addition, the red band is the most heterogeneous one, and the largest intraclass reflectance variability reaches 49%.

Although EM slightly outperformed IM, both of them could obviously reduce the reflectance variability for each class. Increased classification accuracy is expected with these topographically corrected reflectances relative to the UNCORR reflectances.

E. Computational Efficiency

Topographic correction is a key component in the preprocessing streamlines to generate a consistent reflectance product. The computational time of topographic correction methods should be as short as possible to ensure operational implementation. The implementation time of IM for the three selected bands in our study area was very short (2.4 s). For EM, we only counted the time for inversion and simulation procedures because the LUT can be established beforehand. Even so, the implementation time was still unacceptable for operational use (21 h, 37 min, and 22.3 s).

V. DISCUSSION

A. Performance Evaluation of Topographic Correction Methods

Previous studies have found that selection of the evaluation criteria influences the evaluation results of topographic correction methods [43]. Consequently, the multicriteria evaluation is commonly recommended to provide a comprehensive evaluation result [15], [17], [22]. Specifically, the following four criteria were employed in this article.

1) Visual inspection provided the first indicator of the correction performance.
2) Dependences of reflectances on the local illumination condition, and
3) Aspect was used to jointly analyze the reduction in the correlation between topography and reflectances.
4) Reduction in intraclass variability revealed the homogenization of variability after topographic correction, which is a prerequisite to improve land cover mapping accuracy.
5) Computational efficiency was used to analyze the operational implementation potential because an operational algorithm should be as efficient as possible.

We acknowledge that uncertainty exists in each of the evaluation criterion. Visual inspection is subjective and relies on the expertise of the performer [43]. The second and third criteria both assume that vegetation type is independent of the topographic factors (local illumination condition and aspect for the second and third criteria, respectively), which is generally not the case in reality [22]. As suggested in [47], residual correlation between reflectances and topographic factors should be expected, even after a perfect topographic correction.

This is the reason why we introduced the analysis of intraclass variability reduction. However, it is difficult to collect high-accuracy land cover maps over mountainous areas, so we used the separated NDVI as a proxy of land cover type as recommended in [38]. Finally, the computational efficiency is dependent on the platform and software used, yet this is not a big problem because we focused on the comparison between IM and EM rather than the absolute computational efficiency.

Using the multicriteria method, we evaluated the topographic effects on Landsat 8 OLI reflectance in different bands. The red band was found to have a wider dynamic range than the green and Nir bands, even after topographic correction [see Figs. 4(d)–(e) and 7)]. In fact, the variability in red reflectance is not only caused by topography but also by many other factors, e.g., vegetation structure and atmospheric condition. In contrast, the Nir band was found to be more homogeneous than the red band (Figs. 4(f) and 7), which may be partially explained by the multiscattering domination of the canopy reflectance in this band, which can homogenize the structural differences existing in different canopies. In addition, the atmospheric effect in the Nir band is small compared to that in the green and red bands. These two factors together amplify the topographic effects in this band, so the correlation between Nir reflectance and local illumination conditions is obvious, consistent with existing studies [17], [38]. Fortunately, the topographic effects in the Nir band could be successfully mediated through both IM and EM.

B. Comparison Between EM and IM

The main difference between PLC and other well-performing topographic correction methods is that no empirical parameter is involved in PLC, i.e., PLC has a solid physical foundation. In contrast to empirical methods, the physical mechanism underlying PLC can be applied to Landsat 8 OLI images acquired in different regions and dates. Therefore, PLC supports temporally continuous and spatially mosaicked applications. However, the two different implementation pathways of PLC, i.e., EM and IM, have their own advantages and disadvantages:

EM is based on the numerical inversion of the canopy reflectance model. EM is by nature an MFM method, and the difference between our EM and similar MFM methods [12]–[14] is that we used the well-validated PLC vegetation reflectance model [18] rather than others. The direct use of the PLC model allows EM to preserve all the physical mechanisms underlying the radiative transfer process over rugged terrain, and therefore, the EM can excellently mediate the topographic effect in Landsat 8 OLI reflectance. The Landsat 8 OLI imagery after EM correction was obviously homogenized [see Figs. 2(a) and 7(b)], and the dependence of reflectances on the local illumination conditions and aspect were nearly completely removed (see the middle columns of Figs. 5 and 6, respectively). However, EM also has some drawbacks inherited from the direct use of the PLC canopy reflectance model. First, EM caused reflectance distortion for nonvegetation pixels (see the middle column of Fig. 3). This result occurred because the PLC canopy reflectance model was developed based on the vegetation radiative transfer mechanism [18] and therefore cannot be directly applied to other land covers. Second, the multiple best solutions method, which was used to mitigate the ill-posed problem of inversion, eliminated some inherent vegetation information, e.g., the vegetation reflectance dynamic range was compressed after EM correction (see the middle column of Fig. 5). Third, the values of EM corrected reflectances were overestimated (see the middle column of Fig. 6). This overestimation may be derived from the relatively rough parameterization of the PLC model (Table I). Our objective was to establish a transferable topographic correction method; therefore, no specific field measurement was incorporated in the parameterization process, and relatively wide dynamic ranges, which are often recommended for biophysical parameter retrieval [33], were adopted. Overall, although the PLC model is of high fidelity in canopy reflectance model simulation, the EM is challenged by the parameterization and ill-posed problems of the PLC models in forward and inverse applications, respectively, which causes the EM to be unable to reconstruct the "true" vegetation inherent reflectance.

In contrast to EM, IM was derived from the mathematical simplification of the PLC model [17]. The simplification endows IM with a very concise form [(8)], yet a solid physical basis remains. The assessment revealed that IM performed slightly worse than EM in topographic effect elimination. The residual topographic effect may originate from the assumption involved in the deduction of IM formulation. However, two obvious advantages of IM over EM make IM have the potential to be employed in preprocessing streamlines to generate radiometrically consistent reflectance products: 1) in addition to topographic correction, IM can reproduce the inherent vegetation reflectance (see Fig. 6 and Table III) without any artifacts (see Fig. 3) and 2) IM is computationally very efficient and therefore can be operationally implemented.

C. Prospects for Future Studies

This article compared the EM and IM implementations of PLC topographic correction methods. The results confirmed that the IM can satisfactorily reduce topographic effects and simultaneously preserve the inherent vegetation reflectance. In addition, the simple form of IM [(7)] ensures its computational efficiency. Overall, IM has the potential to be operationally used to generate consistent reflectance over mountainous regions. Several steps to improve the IM for facilitating its operationality remain.

First, the IM can successfully convert the bidirectional reflectance distribution function (BRDF) for an inclined surface to its counterpart over a horizontal surface. Slope-caused BRDF distortion is often referred to as the local-scale topographic effect [48]. However, topography also has several nonlocal effects, e.g., the occlusion of direct solar radiance and sky diffuse radiance by adjacent slopes and the addition of diffuse radiance reflected from adjacent slopes [49]. Combined correction for local and nonlocal topographic effects has been proposed in a few studies [37], [38], [50], yet for local-scale topographic effects, these studies only considered the

variation in sun-target-sensor geometry, neglecting the slope-caused BRDF distortion. A combination of IM and existing methods accounting for nonlocal topographic effects will be implemented in our future study to further improve topographic correction.

Second, except for topography, many other factors, including BRDF and atmospheric effects, would perturb the observed signal and reduce reflectance consistency. Currently, the combined correction for BRDF and atmospheric effects has been achieved [51]. Considering the maturity of the atmospheric correction method and the simplicity of Roy's [52] and IM methods for BRDF and topographic correction, respectively, a more comprehensive radiometric calibration is feasible to combine the atmospheric, BRDF, and topographic correction. This method will significantly facilitate the generation of radiometrically consistent reflectances.

Third, IM has undergone extensive assessment against Landsat imagery. The applicability for other similar data sources, e.g., Sentinel 2 MSI, should be assessed in our future work.

Finally, IM and EM are both derived from a vegetation radiative transfer model, and uncertainty arises when they are directly applied to nonvegetation areas. However, the novel paradigm of topographic correction based on numerical inverse and/or analytical approximation of the radiative transfer model can also be applied to other land covers. Therefore, we will develop topographic correction methods for other typical land covers, e.g., soil and snow, with the support of corresponding radiative transfer models.

VI. Conclusion

PLC is a novel topographic correction method with a solid physical basis and high performance. This article compared the two implementation pathways of PLC, i.e., EM and IM, for Landsat 8 OLI imagery. The results showed that both EM and IM could significantly reduce the topographic effects on Landsat 8 OLI vegetation reflectances. EM performed slightly better than IM in eliminating the correlation between topographic characteristics (specifically, local illumination condition and aspect, in this article) and vegetation reflectances. However, the PLC model inversion process involved in EM cannot fully reproduce the inherent vegetation reflectance, and the normalized reflectances overestimated the inherent values. IM does not have this problem because it is based on the analytical approximation of the PLC model, avoiding the numerical inverse process. Therefore, we highlight that IM achieves an appropriate tradeoff between topographic effect elimination and inherent vegetation reflectance preservation. In addition, IM is very computationally efficient. IM will significantly contribute to the generation of radiometrically consistent Landsat 8 OLI vegetation reflectances in support of temporally continuous and spatially mosaicked applications.

References

[1] D. P. Roy *et al.*, "Landsat-8: Science and product vision for terrestrial global change research," *Remote Sens. Environ.*, vol. 145, pp. 154–172, Apr. 2014.

[2] M. A. Wulder *et al.*, "Current status of Landsat program, science, and applications," *Remote Sens. Environ.*, vol. 225, pp. 127–147, May 2019.

[3] G. Yan *et al.*, "Temporal extrapolation of daily downward shortwave radiation over cloud-free rugged Terrains.—Part 1: Analysis of topographic effects," *IEEE Trans. Geosci. Remote Sens.*, vol. 56, no. 11, pp. 6375–6394, Nov. 2018.

[4] S. Qiu, Y. Lin, R. Shang, J. Zhang, L. Ma, and Z. Zhu, "Making landsat time series consistent: Evaluating and improving landsat analysis ready data," *Remote Sens.*, vol. 11, no. 1, p. 51, 2018.

[5] J. A. Smith, T. L. Lin, and K. J. Ranson, "The Lambertian assumption and Landsat data," *Photogramm. Eng. Remote Sens.*, vol. 46, pp. 1183–1189, Sep. 1980.

[6] P. M. Teillet, B. Guindon, and D. G. Goodenough, "On the slope-aspect correction of multispectral scanner data," *Can. J. Remote Sens.*, vol. 8, no. 2, pp. 84–106, Dec. 1982.

[7] D. Gu and A. Gillespie, "Topographic normalization of landsat TM images of forest based on subpixel Sun–Canopy–Sensor geometry," *Remote Sens. Environ.*, vol. 64, no. 2, pp. 166–175, May 1998.

[8] S. A. Soenen, D. R. Peddle, and C. A. Coburn, "SCS+C: A modified Sun-canopy-sensor topographic correction in forested terrain," *IEEE Trans. Geosci. Remote Sens.*, vol. 43, no. 9, pp. 2148–2159, Sep. 2005.

[9] J. R. Dymond and J. D. Shepherd, "Correction of the topographic effect in remote sensing," *IEEE Trans. Geosci. Remote Sens.*, vol. 37, no. 5, pp. 2618–2619, Sep. 1999.

[10] H. Ge, D. Lu, S. He, A. Xu, G. Zhou, and H. Du, "Pixel-based minnaert correction method for reducing topographic effects on a landsat 7 ETM+ image," *Photogramm. Eng. Remote Sens.*, vol. 74, no. 11, pp. 1343–1350, Nov. 2008.

[11] B. Tan *et al.*, "Improved forest change detection with terrain illumination corrected landsat images," *Remote Sens. Environ.*, vol. 136, pp. 469–483, Sep. 2013.

[12] S. Couturier, J.-P. Gastellu-Etchegorry, E. Martin, and P. Patino, "Building a forward-mode three-dimensional reflectance model for topographic normalization of high-resolution (1–5 m) imagery: Validation phase in a forested environment," *IEEE Trans. Geosci. Remote Sens.*, vol. 51, no. 7, pp. 3910–3921, Jul. 2013.

[13] W. Fan *et al.*, "Topographic correction of forest image data based on the canopy reflectance model for sloping terrains in multiple forward mode," *Remote Sens.*, vol. 10, no. 5, p. 717, 2018.

[14] S. A. Soenen, D. R. Peddle, C. A. Coburn, R. J. Hall, and F. G. Hall, "Improved topographic correction of forest image data using a 3-D canopy reflectance model in multiple forward mode," *Int. J. Remote Sens.*, vol. 29, no. 4, pp. 1007–1027, Feb. 2008.

[15] K. Hurni, J. Van Den Hoek, and J. Fox, "Assessing the spatial, spectral, and temporal consistency of topographically corrected landsat time series composites across the mountainous forests of nepal," *Remote Sens. Environ.*, vol. 231, Sep. 2019, Art. no. 111225.

[16] H. Reese and H. Olsson, "C-correction of optical satellite data over alpine vegetation areas: A comparison of sampling strategies for determining the empirical c-parameter," *Remote Sens. Environ.*, vol. 115, no. 6, pp. 1387–1400, Jun. 2011.

[17] G. Yin *et al.*, "PLC: A simple and semi-physical topographic correction method for vegetation canopies based on path length correction," *Remote Sens. Environ.*, vol. 215, pp. 184–198, Sep. 2018.

[18] G. Yin, A. Li, W. Zhao, H. Jin, J. Bian, and S. Wu, "Modeling canopy reflectance over sloping terrain based on path length correction," *IEEE Trans. Geosci. Remote Sens.*, vol. 55, no. 8, pp. 4597–4609, Aug. 2017.

[19] G. Yin *et al.*, "Path length correction for improving leaf area index measurements over sloping terrains: A deep analysis through computer simulation," *IEEE Trans. Geosci. Remote Sens.*, early access, Jan. 30, 2020, doi: 10.1109/TGRS.2019.2963366.

[20] R. A. Duursma, J. D. Marshall, and A. P. Robinson, "Leaf area index inferred from solar beam transmission in mixed conifer forests on complex terrain," *Agricult. Forest Meteorol.*, vol. 118, nos. 3–4, pp. 221–236, Sep. 2003.

[21] E. María Luisa, B. Frédéric, and W. Marie, "Slope correction for LAI estimation from gap fraction measurements," *Agricult. Forest Meteorol.*, vol. 148, no. 10, pp. 1553–1562, Sep. 2008.

[22] I. Sola, M. González-Audícana, and J. Álvarez-Mozos, "Multi-criteria evaluation of topographic correction methods," *Remote Sens. Environ.*, vol. 184, pp. 247–262, Oct. 2016.

[23] Y. V. Knyazikhin, A. L. Marshak, and R. B. Myneni, "Interaction of photons in a canopy of finite-dimensional leaves," *Remote Sens. Environ.*, vol. 39, no. 1, pp. 61–74, Jan. 1992.

[24] R. B. Myneni, A. L. Marshak, and Y. V. Knyazikhin, "Transport-theory for a leaf canopy of finite-dimensional scattering centers," *J. Quant. Spectrosc. Radiat. Transf.*, vol. 46, pp. 259–280, Oct. 1991.
[25] A. Kuusk, "A fast, invertible canopy reflectance model," *Remote Sens. Environ.*, vol. 51, no. 3, pp. 342–350, Mar. 1995.
[26] Y. Zeng *et al.*, "A radiative transfer model for heterogeneous AGROforestry scenarios," *IEEE Trans. Geosci. Remote Sens.*, vol. 54, no. 8, pp. 4613–4628, Aug. 2016.
[27] Y. Zeng *et al.*, "Spectral invariant provides a practical modeling approach for future biophysical variable estimations," *Remote Sens.*, vol. 10, no. 10, p. 1508, 2018.
[28] Y. Zeng *et al.*, "Extracting leaf area index by sunlit foliage component from downward-looking digital photography under clear-sky conditions," *Remote Sens.*, vol. 7, no. 10, pp. 13410–13435, 2015.
[29] C. B. Schaaf, X. Li, and A. H. Strahler, "Topographic effects on bidirectional and hemispherical reflectances calculated with a geometric-optical canopy model," *IEEE Trans. Geosci. Remote Sens.*, vol. 32, no. 6, pp. 1186–1193, Nov. 1994.
[30] J.-P. Gastellu-Etchegorry *et al.*, "Discrete anisotropic radiative transfer (DART 5) for modeling airborne and satellite spectroradiometer and LIDAR acquisitions of natural and urban landscapes," *Remote Sens.*, vol. 7, no. 2, pp. 1667–1701, 2015.
[31] W. Fan, J. M. Chen, W. Ju, and G. Zhu, "GOST: A geometric-optical model for sloping terrains," *IEEE Trans. Geosci. Remote Sens.*, vol. 52, no. 9, pp. 5469–5482, Sep. 2014.
[32] S. Jacquemoud *et al.*, "PROSPECT+SAIL models: A review of use for vegetation characterization," *Remote Sens. Environ.*, vol. 113, pp. S56–S66, Sep. 2009.
[33] F. J. García-Haro *et al.*, "Derivation of global vegetation biophysical parameters from EUMETSAT polar system," *ISPRS J. Photogramm. Remote Sens.*, vol. 139, pp. 57–74, May 2018.
[34] B. Combal *et al.*, "Retrieval of canopy biophysical variables from bidirectional reflectance - Using prior information to solve the ill-posed inverse problem," *Remote Sens. Environ.*, vol. 84, pp. 1–15, Jan. 2003.
[35] X. Quan, B. He, and X. Li, "A Bayesian network-based method to alleviate the ill-posed inverse problem: A case study on leaf area index and canopy water content retrieval," *IEEE Trans. Geosci. Remote Sens.*, vol. 53, no. 12, pp. 6507–6517, Dec. 2015.
[36] S. Wu *et al.*, "The definition of remotely sensed reflectance quantities suitable for rugged terrain," *Remote Sens. Environ.*, vol. 225, pp. 403–415, May 2019.
[37] J. Wen *et al.*, "Modeling land surface reflectance coupled BRDF for HJ-1/CCD data of rugged terrain in heihe river basin, China," *IEEE J. Sel. Topics Appl. Earth Observ. Remote Sens.*, vol. 8, no. 4, pp. 1506–1518, Apr. 2015.
[38] F. Li *et al.*, "A physics-based atmospheric and BRDF correction for landsat data over mountainous terrain," *Remote Sens. Environ.*, vol. 124, pp. 756–770, Sep. 2012.
[39] S. Wang, W. Chen, and J. Cihlar, "New calculation methods of diurnal distribution of solar radiation and its interception by canopy over complex terrain," *Ecol. Model.*, vol. 155, nos. 2–3, pp. 191–204, Oct. 2002.
[40] J. Wen *et al.*, "Characterizing land surface anisotropic reflectance over rugged terrain: A review of concepts and recent developments," *Remote Sens.*, vol. 10, no. 3, p. 370, 2018.
[41] *Landsat 8 (L8) Data Users Handbook*, USGS, Reston, VA, USA, 2018.
[42] T. Tachikawa, M. Hato, M. Kaku, and A. Iwasaki, "Characteristics of ASTER GDEM version 2," in *Proc. IEEE Int. Geosci. Remote Sens. Symp.*, New York, NY, USA, Jul. 2011, pp. 3657–3660.
[43] I. Sola, M. Gonzalez-Audicana, J. Alvarez-Mozos, and J. L. Torres, "Synthetic images for evaluating topographic correction algorithms," *IEEE Trans. Geosci. Remote Sens.*, vol. 52, no. 3, pp. 1799–1810, Mar. 2014.
[44] S. R. Hale and B. N. Rock, "Impact of topographic normalization on land-cover classification accuracy," *Photogramm. Eng. Remote Sens.*, vol. 69, no. 7, pp. 785–791, Jul. 2003.
[45] G. Yin, A. Li, and A. Verger, "Spatiotemporally representative and cost-efficient sampling design for validation activities in wanglang experimental site," *Remote Sens.*, vol. 9, no. 12, p. 1217, 2017.
[46] V. Balthazar, V. Vanacker, and E. F. Lambin, "Evaluation and parameterization of ATCOR3 topographic correction method for forest cover mapping in mountain areas," *Int. J. Appl. Earth Observ. Geoinf.*, vol. 18, pp. 436–450, Aug. 2012.
[47] S. Hantson and E. Chuvieco, "Evaluation of different topographic correction methods for landsat imagery," *Int. J. Appl. Earth Observ. Geoinformation*, vol. 13, no. 5, pp. 691–700, Oct. 2011.
[48] J. A. Ruiz-Arias, T. Cebecauer, J. Tovar-Pescador, and M. Šúri, "Spatial disaggregation of satellite-derived irradiance using a high-resolution digital elevation model," *Sol. Energy*, vol. 84, no. 9, pp. 1644–1657, Sep. 2010.
[49] A. Mousivand, W. Verhoef, M. Menenti, and B. Gorte, "Modeling top of atmosphere radiance over heterogeneous non-Lambertian rugged terrain," *Remote Sens.*, vol. 7, no. 6, pp. 8019–8044, 2015.
[50] K. Yu, S. Liu, and Y. Zhao, "CPBAC: A quick atmospheric correction method using the topographic information," *Remote Sens. Environ.*, vol. 186, pp. 262–274, Dec. 2016.
[51] N. Flood, T. Danaher, T. Gill, and S. Gillingham, "An operational scheme for deriving standardised surface reflectance from landsat TM/ETM+ and SPOT HRG imagery for eastern australia," *Remote Sens.*, vol. 5, no. 1, pp. 83–109, 2013.
[52] D. P. Roy *et al.*, "A general method to normalize landsat reflectance data to nadir BRDF adjusted reflectance," *Remote Sens. Environ.*, vol. 176, pp. 255–271, Apr. 2016.

Gaofei Yin (Member, IEEE) received the Ph.D. degree from the Institute of Remote Sensing and Digital Earth, Chinese Academy of Sciences, Beijing, China, in 2015.

From 2015 to 2018, he was with the Institute of Mountain Hazards and Environment, Chinese Academy of Sciences, Chengdu, China. Since 2018, he has been an Associate Professor with the Faculty of Geosciences and Environmental Engineering, Southwest Jiaotong University, Chengdu, also a Marie Skłodowska-Curie Individual Fellow with the Global Ecology Unit, Center for Ecological Research and Forestry Applications, Barcelona, Spain. His research interests include canopy reflectance modeling, biophysical variables estimation, and climate–vegetation dynamics.

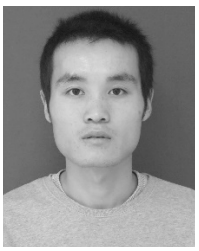

Lei Ma received the M.Sc. degree in geographic information system from Southwest Jiaotong University, Chengdu, China, in 2011, and the Ph.D. degree in geography from Nanjing University, Nanjing, China, in 2016.

From 2016 to 2019, he was a Research Associate with Nanjing University. He was also a Post-Doctoral Research Fellow with Texas Tech University, Lubbock, Texas, USA, from 2018 to 2019. Since 2019, he has been an Alexander von Humboldt Research Fellow with the Technical University of Munich and an Associate Professor with Nanjing University. His research interests include object-based image analysis, land cover and land use change, high-resolution image analysis, and time series analysis. He received the Jack Dangermond Award–Best Paper 2017 in 2019 and the Jiangsu Province-level outstanding Diploma thesis award in 2017. He is a Guest Editor of Remote Sensing

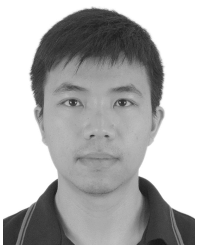

Wei Zhao (Senior Member, IEEE) received the B.S. degree in geographic information system from Beijing Normal University, Beijing, China, in 2006 and the Ph.D. degree in cartography and geographic information system from the Institute of Geographic Sciences and Natural Resources Research, Chinese Academy of Sciences (CAS), Beijing, China, in 2012.

From 2012 to 2015, he was a Research Assistant with the Institute of Mountain Hazards and Environment (IMHE), CAS, Chengdu, China. Currently, he is an Associate Professor with IMHE. His research field is mountain quantitative remote sensing with special focuses on land surface energy fluxes and soil moisture estimation, spatial scale effect on remote sensing data, terrain effect correction, and thermal environment monitoring.

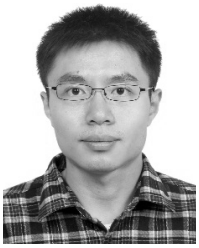

Yelu Zeng (Member, IEEE) received the B.S. degree in remote sensing from Wuhan University, Wuhan, China, in 2011, and the Ph.D. degree from the Institute of Remote Sensing and Digital Earth, Chinese Academy of Sciences, Beijing, China, in 2016.

He is currently a Post-doctoral Fellow with the Carnegie Institution for Science in Stanford, CA, USA. His research interests include 3-D radiative transfer modeling over vegetation canopies and solar-induced chlorophyll fluorescence (SIF).

Baodong Xu received the Ph.D. degree from the Institute of Remote Sensing and Digital Earth, Chinese Academy of Sciences, Beijing, China, in 2018. Since 2018, he has been an Associate Professor with the Macro Agriculture Research Institute, College of Resources and Environment, Huazhong Agricultural University, Wuhan, China. His current research interests include biophysical variables estimation, validation of remote sensing products, and remote sensing applications in agriculture.

Shengbiao Wu received the B.S. degree in base class of geography at Wuhan University in 2013, and the Ph.D. degree from the Aerospace Information Research Institute, Chinese Academy of Sciences, Beijing, China, in 2019. He is currently a Postdoctoral Fellow with the Faculty of Science, University of Hong Kong since September 2019. His research mainly focused on the vegetation radiative transfer, surface biophysical parameter retrieval, land surface energy budget, and plant phenology diversity.